

# Numerical and experimental study of the wave-induced free surface boundary layer in a canal

M. Baklouti<sup>1,3</sup>, O. Kimmoun<sup>1</sup>, B. Molin<sup>1</sup>, L. Gentaz<sup>2</sup>, B. Alessandrini<sup>2</sup>

<sup>1</sup> Ecole Supérieure d'Ingénieurs de Marseille      <sup>2</sup> Ecole Centrale de Nantes

<sup>3</sup> Laboratoire des Sciences du Génie Chimique, CNRS-UPR 6811, Nancy

## 1. Introduction

Since the work of Stokes, it is well-known that, in water waves, particles of inviscid fluid possess a steady second-order drift velocity in the direction of wave advance. In small amplitude regular waves, the drift velocity is given as

$$\overline{U}_L(z) = \frac{1}{2} k A^2 \omega \frac{\cosh 2k(z+h)}{\sinh^2 kh} \quad (1)$$

where  $A$  is the wave amplitude,  $\omega$  the frequency,  $k$  the wave number,  $h$  the water depth and  $z$  the vertical coordinate ( $z = 0$  being the undisturbed free surface, and  $z$  pointing upwards).

In a finite length canal, the associated mass transport is being compensated by a return current. For a long tank, and in inviscid fluid, it is a uniform flow with velocity

$$U_R(z) = -\frac{1}{2} \frac{A^2 \omega}{h} \coth kh \quad (2)$$

In a viscous fluid boundary layers appear at the free surface and at the bottom. To first-order in the wave steepness  $kA$  they are oscillatory boundary layers, with thicknesses  $O(\sqrt{\nu/\omega})$ , that is in our experiments where  $\omega = 2\pi$  rd/s, less than one millimeter.

In 1953, Longuet-Higgins (see also Mei, 1983, ch 9) provided a second-order analysis of the free surface and bottom boundary layers. He obtained the remarkable result that steady effects are induced at the outer edges of the oscillatory boundary layers. At the bottom it is a steady drift velocity, while at the free surface it is a steady shear, given by

$$\left. \frac{\partial \overline{U}}{\partial z} \right|_{z=0} = 2 k^2 A^2 \omega \coth kh \quad (3)$$

equal to, and supplementing, the vertical gradient of the Stokes drift (1). An experimental confirmation of this result was provided by Longuet-Higgins (1960).

When regular waves are being produced from  $t = 0$ , this free surface shear should cause a forward current within an outer boundary layer of growing thickness  $O(\sqrt{\nu t})$ . From the diffusion equation one obtains the expression (Longuet-Higgins, 1992)

$$\overline{U}(z, t) = 4 \sqrt{\frac{\nu t}{\pi}} k^2 A^2 \omega \coth kh f(z/2\sqrt{\nu t}), \quad f(\zeta) = e^{-\zeta^2} + 2\zeta \int_{-\infty}^{\zeta} e^{-\eta^2} d\eta \quad (4)$$

When the waves stop at  $t = t_{\text{end}}$ , the profile of the free surface current at subsequent times can be obtained from the diffusion equation with  $\partial \overline{U} / \partial z = 0$  at  $z = 0$  and matching with  $\overline{U}(z, t_{\text{end}})$ . Thus one would expect to observe a free surface residual current of thickness  $O(\sqrt{\nu t})$ , in the wave direction, decreasing in time.

Visual observations in the wave tanks of ESIM and ECN have given the opposite! After tests in regular waves residual currents are actually observed at the free surface, a few millimeters thick, but flowing in the wrong direction, that is from the beach toward the wavemaker.

This contradiction has motivated the present study, where we have combined PIV measurements and numerical simulations with a Navier-Stokes solver. The two investigations are briefly reported in the following.

## 2. PIV measurements

The experiments were performed in the ESIM tank, which is 16.77 m long and 0.65 m wide, at a water depth of 0.79 m. The wavemaker is of flap type, with its axis of rotation about 40 cm below the tank floor. All the walls, floor included, are in glass.

The tests consisted in producing trains of regular waves with the same period of 1 s, but varying amplitudes and numbers of cycles. Velocity measurements were done after the waves had been produced and the tank was going back to rest, in a 10 cm x 10 cm window at about 5.5 m from the wavemaker.

Figure 1 gives an example of measured velocity profiles after 80 cycles of a 5 cm amplitude regular wave train. Times in the figure refer to the instant the wavemaker has been switched off. Velocities around 1 cm/s are obtained at the free surface, toward the wavemaker. A reverse flow appears immediately below.

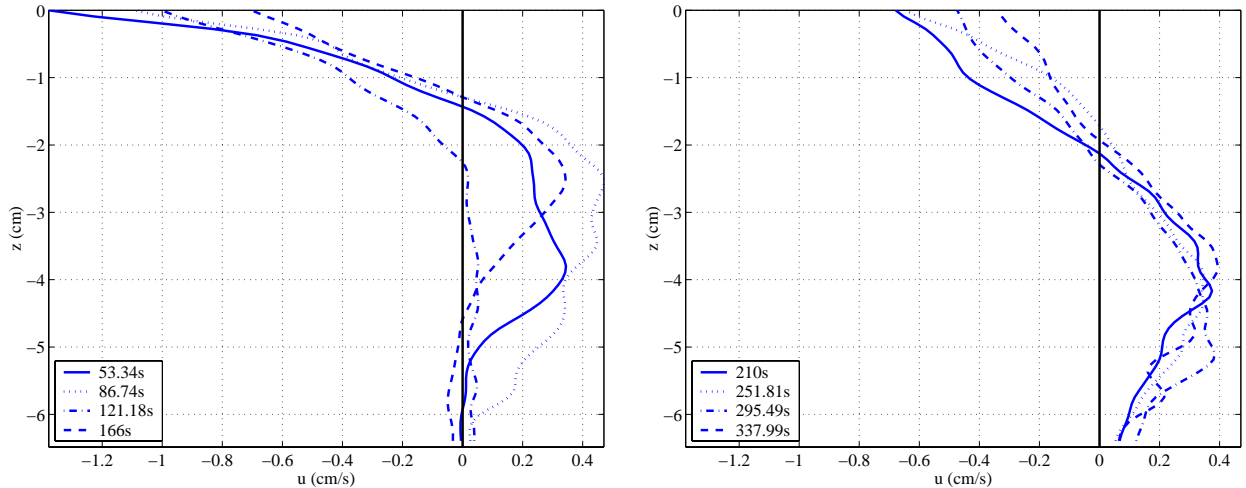


Figure 1. Measured residual current at the free surface after 80 cycles of 5 cm amplitude waves.

As the lack of coherence of these profiles suggests, the accuracy of our measurements cannot be deemed to be very good. At small wave amplitudes (1 or 2 cm) it was not possible to extract coherent values, nor even to visually determine whether there was any free surface current at all. At larger wave amplitudes, it was always observed to flow toward the wavemaker. At a given wave amplitude, the current velocity increases with the number of cycles, until some asymptotic value has been reached. The number of cycles to reach the asymptotic value decreases with increasing wave amplitude.

### 3. Numerical simulations

#### 3.1 The numerical model

The numerical model, *ICARE*, was developed by L. Gentaz during his PhD thesis (Gentaz, 1995). It is a 2D Navier-Stokes solver that models the laminar flow of an incompressible fluid with a free surface. Adaptive meshing is applied to track the free surface.

The continuity and momentum equations are discretized to second order in time and space, using finite difference schemes. The resultant sparse implicit linear system (the unknowns being the velocity components, the pressure and the free surface elevation) is solved by a CGSTAB algorithm, with some iterations on non-linearities at each time step. This coupled resolution ensures a great convergence rate of non-linearities as well as an accurate unsteady free surface flow computation. Further details can be found in Gentaz *et al.* (1998), where *ICARE* is successfully applied to the propagation of waves in the ECN wave tank.

#### 3.2 Application to the ESIM tank

In the numerical model the geometry is divided in three sub-domains. In the first sub-domain, extending about 50 cm from the wavemaker, the nodes are allowed to move both horizontally and vertically, in order to adjust to the motion of the wavemaker. The second sub-domain extends over the next 12 m, and corresponds to the "working section" of the physical tank. In this sub-domain the nodes move only vertically. Their vertical position is related to the free surface elevation  $\eta(x, t)$  through the affine relationship

$$z_j(x_i, t) = z_{j0} + \eta(x_i, t) \frac{z_{j0} + h}{h} \quad (5)$$

where  $z_{j0}$  is the reference position at rest.

The third sub-domain is the numerical beach, where the horizontal mesh size is gradually increased so that waves get dissipated. The length of the numerical beach thus achieved is about 105 m, much longer than the physical one (5 m). An Orlanski condition is applied at the far right boundary to let long waves with velocity  $\sqrt{gh}$  propagate out of the domain. This is another difference with the physical tank where the long waves get reflected by the end-wall.

The horizontal mesh size, in sub-domains 1 and 2, is equal to 3.1 cm (one fiftieth of the wavelength), while the vertical mesh size varies from about 2.5 cm, in the bulk of the fluid, down to less than 0.1 mm by the free surface, in order to properly model the oscillatory boundary layer (the kinematic viscosity  $\nu$  is taken equal to  $10^{-6} \text{ m}^2\text{s}^{-1}$  in the computations).

The total number of nodes is 400 x 90 in the working section, plus 80 x 90 in the numerical beach, that is slightly over 43 000 nodes.

### 3.3 Validation of the numerical model

The main concern was the ability of *ICARE* to properly represent the boundary layer effects, at such low values of the kinematic viscosity and for such a deformed vertical grid: in the bulk of the tank, the mesh size is 3.1 cm x 2.5 cm, while it is 3.1 cm x 0.004 cm at the free surface. Such a variation in the vertical mesh size is likely to induce numerical dissipation, with the risk that unrealistic boundary layers would be obtained.

#### 3.3.a Bottom boundary layer

As a first check, we focused on the bottom boundary layer. According to Longuet-Higgins (1953), the first-order horizontal velocity by the bottom is given by

$$u_1(x, z, t) = \frac{A\omega}{\sinh kh} \left[ \cos(kx - \omega t) - e^{-(z+h)/\delta} \cos\left(kx + \frac{z+h}{\delta} - \omega t\right) \right] \quad (6)$$

with  $\delta = \sqrt{2\nu/\omega}$ , while the mean induced second-order velocity is

$$\bar{u}_2(z) = \frac{k A^2 \omega}{4 \sinh^2 kh} (3 + 3 e^{-2\eta} - 8 \cos \eta e^{-\eta}) \quad (7)$$

and  $\eta = (z+h)/\delta$ . Equation (7) excludes the effects of the lagrangian drift (1) and of the return current (2) and assumes that a steady state has been reached, that is to make comparisons with *ICARE* the simulation time must be large as compared to  $(z+h)^2/\nu$ .

When post-processing the results obtained with *ICARE* and deriving time-averaged values, we must be careful that the obtained velocities refer to pseudo-lagrangian markers which are moving vertically only, according to (5). This means that the associated pseudo-lagrangian mean velocity is not given by (1), but by

$$\bar{U}_{PL}(z) = \frac{k A^2 \omega}{2h} (z+h) \frac{\sinh k(z+h)}{\sinh kh} \quad (8)$$

and is therefore zero at the bottom.

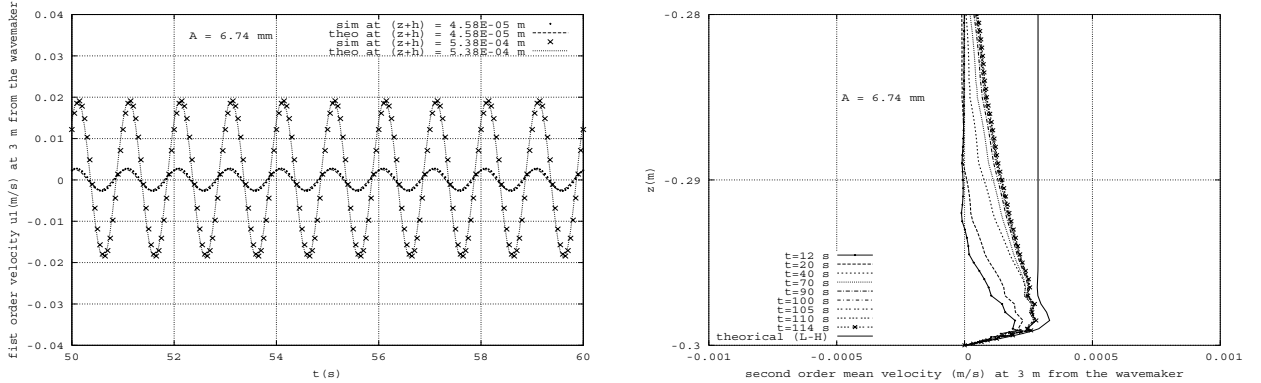


Figure 2. Left (a): time traces of the horizontal velocity at the bottom, compared with L-H's model. Right(b): time-averaged velocity profiles.

Calculations were done with a reduced water depth of 30 cm, at a wave amplitude of 0.67 cm. Figure 2 (a) shows a comparison between numerical and analytical values of the oscillatory horizontal velocity, at two values of  $z+h$  (0.00458 cm and 0.0538 cm), with a good agreement. In figure 2 (b), mean velocity profiles are given at different times. The numerical values have been obtained through time-averaging over windows one period long, and removal of the return current contribution, applying the Stokes model of the flat plate in impulsive flow. That is, we consider that the return current gets established at time  $t_0 = x/C_G$  after the wavemaker has been switched on, ( $C_G$  being the group velocity), and that the velocity profile in the boundary layer is given by

$$U_R(z) = -\frac{1}{2} \frac{A^2 \omega}{h} \coth kh \operatorname{erf} \left( \frac{z+h}{2\sqrt{\nu(t-t_0)}} \right) \quad (9)$$

"erf" being the "error" function. It can be observed that the numerical profiles do tend toward the theoretical one (7) as time increases, albeit there seems to be some under-shoot at the location of the maximum.

#### 3.3.b First-order oscillatory vorticity at the free surface

According to Longuet-Higgins (1953), the first-order oscillatory vorticity at the free surface has the following modulus

$$\Omega(z) = 2k A \omega e^{z/\delta} \quad (10)$$

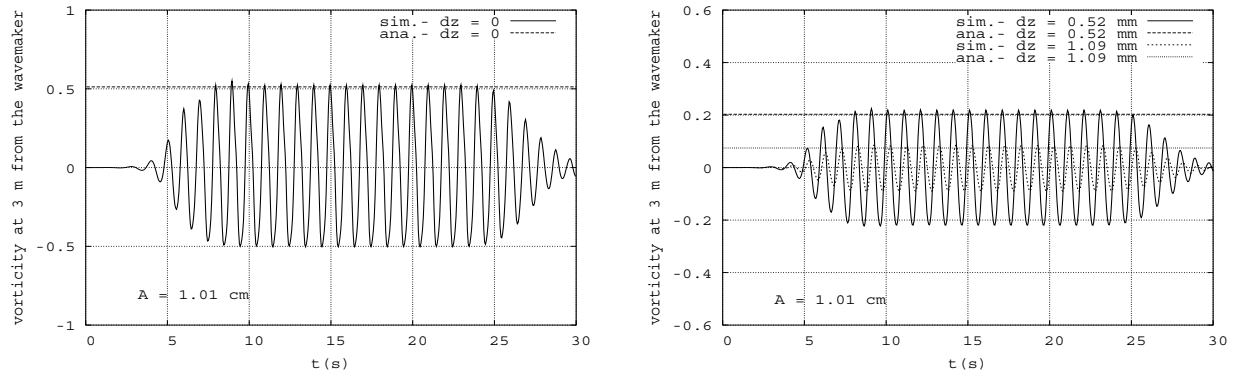


Figure 3. Time traces of the vorticity at the free surface (left) and within the free surface boundary layer (right).

In fig. 3 we show time traces of the vorticity, as derived from the *ICARE* simulations, at the free surface (left), and slightly below (right), within the oscillatory boundary layer, at  $z = -0.52$  mm and  $z = -1.09$  mm. The wave amplitude is 1.01 cm and the number of cycles is 25, including two ramps of 5 cycles at the start and at the end. It can be seen that the agreement with the theoretical values (shown as horizontal lines) is excellent. This proves that numerical dissipation does not occur in our simulations.

### 3.4 Mean velocity at the free surface

Finally we present numerical values of the mean velocity profile by the free surface, for two wave amplitudes of 0.52 cm (fig. 4a) and 3.3 cm (fig. 4b). They are given at different times ( $t = 0$  being the start of the wavemaker motion) and are obtained by averaging the velocity over one period. For a reference, the inviscid profile, as obtained by adding (8) and (2), is given. At the smaller wave amplitude, it can be seen that the numerical and theoretical profiles agree well at submergences larger than 1 cm, and that the numerical profile deviates toward the right (down-wave) over the first centimeter. Moreover the slope at the free surface agrees well with Longuet-Higgins' value (3) (after removing the pseudo-lagrangian drift contribution (8)): equation (3) gives  $0.0055 \text{ s}^{-1}$  while from the numerical simulations we get  $0.0052 \text{ s}^{-1}$ .

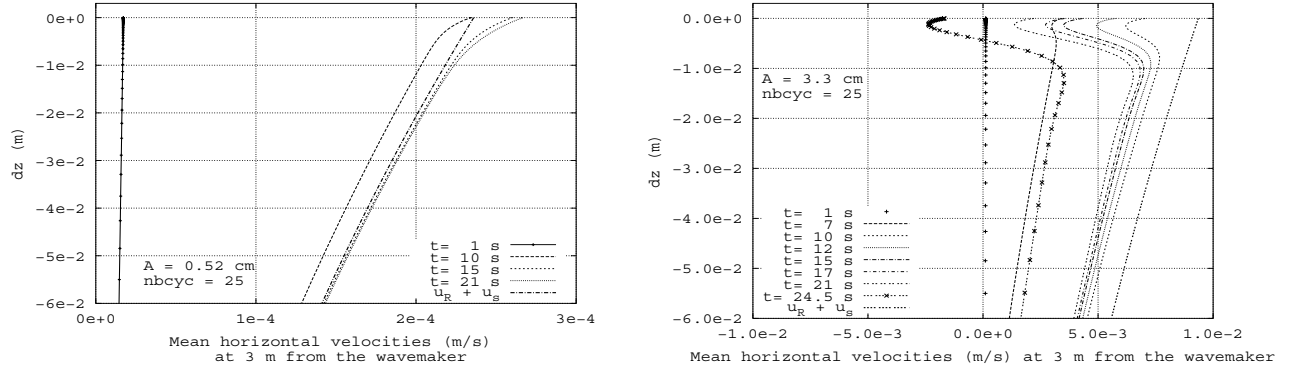


Figure 4. Time averaged velocity profiles by the free surface. Wave amplitudes of 0.5 cm (left) and 3.3 cm (right).

At the larger wave amplitude, even though the slope at the free surface is still positive, the flow reverses to the left. The numerical velocities and profiles are in qualitative agreement with the experimental observations.

## References

- GENTAZ L. 1995 Simulation bi-dimensionnelle en fluide visqueux de la propagation d'ondes de gravité et du mouvement forcé d'un corps : résolution des équations de Navier-Stokes en présence d'une surface libre, PhD thesis report, Nantes (in French).
- GENTAZ L., MAURY C., ALESSANDRINI B. & DELHOMMEAU G. 1998 Numerical simulation of a two-dimensional wave tank in viscous fluid, *Proc. ISOPE Conf.*, Vol.III, 256-263.
- LONGUET-HIGGINS M.S. 1953 Mass transport in water waves, *Phil. Trans. R. Soc. Lond. A*, **245**, 535-581.
- LONGUET-HIGGINS M.S. 1960 Mass transport in the boundary layer at a free oscillating surface, *J. Fluid Mech.*, **8**, 293-306.
- LONGUET-HIGGINS M.S. 1992 Capillary rollers and bores, *J. Fluid Mech.*, **240**, 659-679.
- MEI C.C. 1983 *The Applied Dynamics of Ocean Surface Waves*, Wiley-Interscience.

**Question by : M. Tulin**

First, congratulations on carrying out these beautiful experimental studies. The behaviour of the flow within a real wavetank is one of the most neglected subjects in the field of wave hydrodynamics, despite its great practical importance. Did you ever find surface flow toward the wavemaker while waves were being generated? I ask this because we have observed this phenomenon in our large UCSB tank, through the use of floating surface particles. My recollection is that this occurs after some time, but not early. It was in any event our practice to make measurements as early as possible after starting the wavemaker, as strong + visible surface disturbances appear later. (See a paper by Tulin & Waseda in JFM, January 1999 I think -- where disturbances are traced and discussed).

**Author's reply:**

Thank you for your comments. We did not try to measure the drift velocity of freely floating particles while the waves were being generated. Maybe we will so in another series of experiments. Your observations seem to be in qualitative accordance with our measurements and calculations.

---

**Questions by : D.H. Peregrine**

1. Did you consider the long waves generated as the set-up on the beach radiates back down the tank, and effects of surfactant layers spreading once waves stop?
2. Longuet-Higgins (1953) mentions both 'conductive' and 'convective' regimes. Which regimes are represented by your experiments?

**Author's reply:**

1. We were aware of the long waves. Their horizontal velocity profiles are nearly constant over the depth, so we eliminated their effect by considering the relative velocity of the upper layer with respect to the fluid a few centimetres below. We did not consider the effects of surfactants.
  2. We believe that we were in the conductive regime. According to the discussion paragraph in Longuet-Higgins' paper, convection comes into play after some time, of order  $L/(A^2 \omega k)$  where  $L$  is the length of the tank. In our experiments the wavemaker was acted for much shorter durations.
-